Supplement of Atmos. Meas. Tech., 12, 4309–4337, 2019
https://doi.org/10.5194/amt-12-4309-2019-supplement

Atmospheric Measurement Techniques
Open Access

Supplement of

Aerosol optical depth comparison between GAW-PFR and AERONET-Cimel radiometers from long-term (2005–2015) 1 min synchronous measurements

Emilio Cuevas et al.

Correspondence to: Emilio Cuevas (ecuevasa@aemet.es)

Supplement S1. One-minute AOD data differences between AERONET-Cimel (V3) and GAW-PFR.

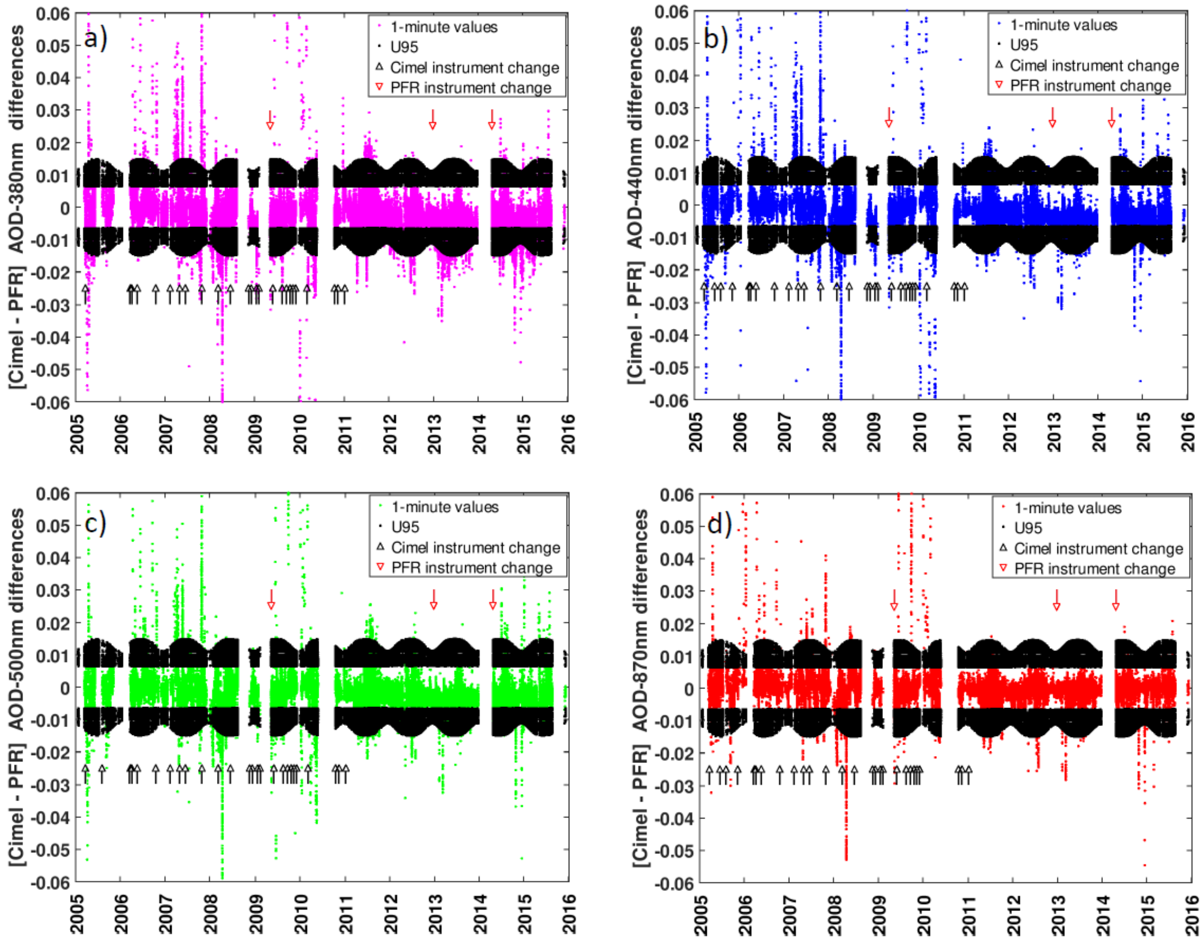

S1. One-minute AOD data differences between AERONET-Cimel (V3) and GAW-PFR for (a) 380 nm (75303 data-pairs), (b) 440 nm (76290 data-pairs), (c) 500 nm (75335 data-pairs) and (d) 870 nm (76307 data-pairs) for the period 2005-2015. Black dots correspond to the U95 limits. A small number of outliers are out of the ±0.06 AOD differences range. Black arrows indicate a change of Reference AERONET-Cimel radiometer and red arrows indicate a change of the GAW-PFR instrument.

Supplement S2. Percentage of [Cimel (V3)-PFR] 1-minute AOD differences meeting the WMO criteria for the four compared channels.

S2.1. Percentage of AERONET-Cimel 1-minute AOD data (V3) meeting the WMO criteria for the four compared channels, and different AOD and AE scenarios for the period 2005-2015, number of data pairs are shown in brackets. The last row corresponds to the total percentages for the sub-period 2010-2015. AOD and AE traceability > 95% are marked in bold. This Table is equivalent to Table 4 of the manuscript for AERONET V2.

% of data within WMO limits	380 nm	440 nm	500 nm	870 nm
AOD≤0.05	93.6 (60264)	**96.3 (62836)**	**97.1 (62545)**	**98.4 (64213)**
0.05<AOD≤0.10	91.0 (5138)	92.0 (5217)	92.6 (5222)	94.7 (5372)
AOD>0.10	77.1 (4085)	84.1 (4537)	81.6 (4326)	93.3 (5034)
AE≤0.25	78.7 (2472)	82.3 (2588)	79.0 (2483)	92.9 (6530)
0.25<AE≤0.6	90.2 (5941)	94.3 (6321)	94.9 (6255)	**97.4 (6530)**
AE>0.6	94.1 (56952)	**96.5 (59181)**	**97.1 (58793)**	**98.7 (60514)**
Total 2005-2015	92.3 (69487)	**95.2 (72590)**	**95.7 (72093)**	**97.8 (74619)**
Total 2010-2015	92.8 (42463)	**96.8 (44328)**	**96.8 (44329)**	**98.8 (44329)**

S2.2 Percentage of AERONET-Cimel 1-minute AOD data (V3) meeting the WMO criteria for optical air mass > 5.0 for the period 2005-2015. The number of data pairs are shown in brackets.

% of data within WMO limits	380 nm	440 nm	500 nm	870 nm
m > 5.0	90.9 (9328)	93.4 (9474)	94.7 (9412)	96.7 (9475)

Supplement S3. AOD variability 1-minute interval.

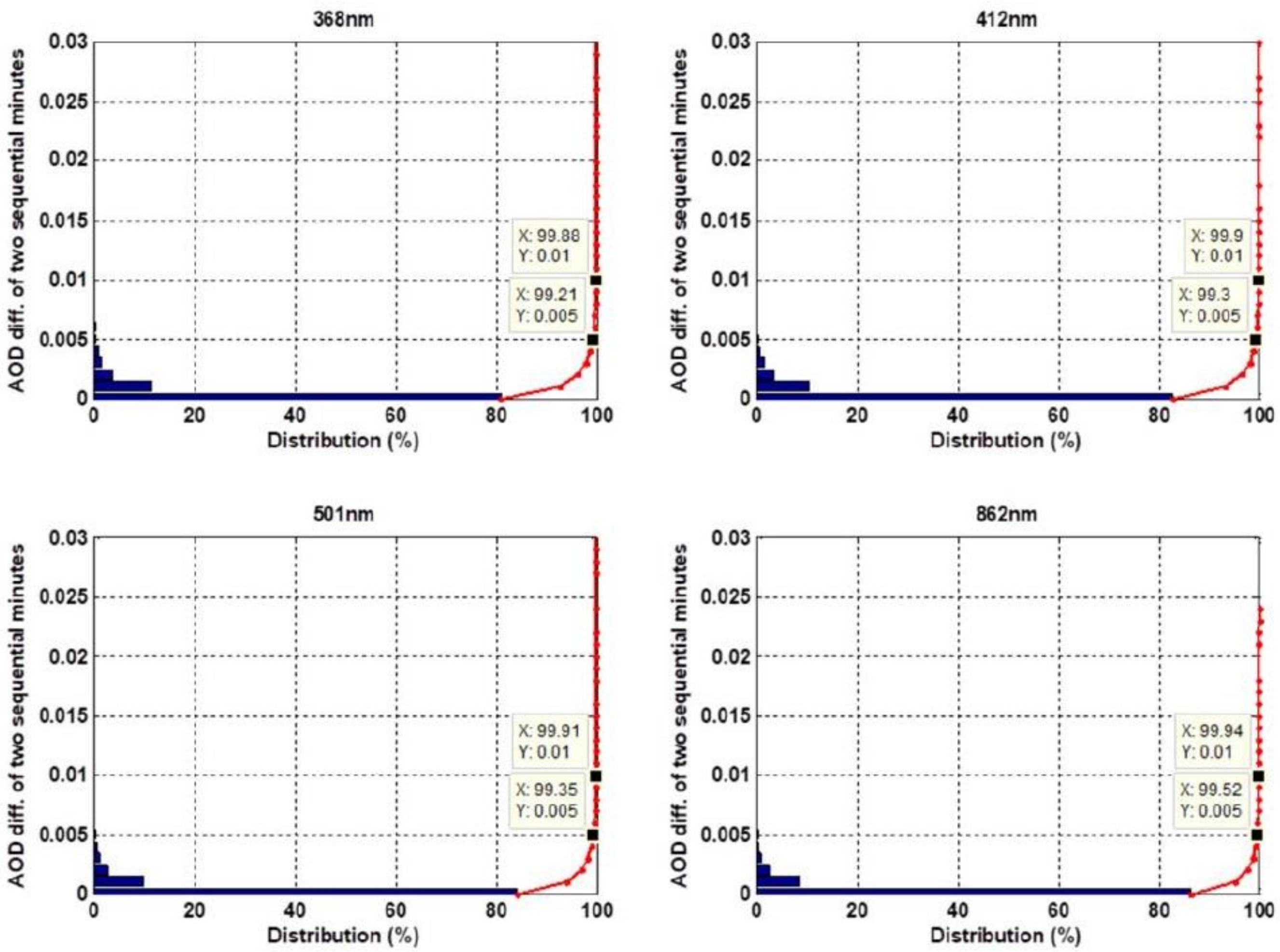

S3.1. Percentage of data with 1-minute AOD variability for the four GAW-PFR channels (368 nm, 412 nm, 501 nm, and 862nm).

S3.2. Percentage of 1-minute AOD data from the Cimel triplets (year 2013) whose range of variation AOD_{max}-AOD_{min} > 0.015, for several AOD intervals, and for 380 nm and 500 nm. This value is half of the WMO traceability interval when m = 1 (maximum possible interval) (see Eq.2 of the manuscript).

380nm: 114 points outside WMO limits

AOD range	# cases outside WMO limit	Total # cases	% in AOD range	% in total # cases
≤ 0.03	13	11800	0.11	$6.5x10^{-4}$
(0.03-0.05]	14	3712	0.38	$7.0x10^{-4}$
(0.05-0.1]	18	1932	0.93	$9.0x10^{-4}$
(0.1-1.0]	61	2637	2.31	0.30
Total [0.0-1.0]	106	20081	0.52	0.52

500nm: 64 points outside WMO limits

AOD range	# cases outside WMO limit	Total # cases	% in AOD range	% in total # cases
≤ 0.03	2	13629	0.01	$9.9x10^{-5}$
(0.03-0.05]	11	2401	0.46	$5.4x10^{-4}$
(0.05-0.1]	9	1600	0.56	$4.5x10^{-4}$
(0.1-1.0]	42	2484	1.69	0.20
Total [0.0-1.0]	64	20114	0.32	0.32

Supplement S4. One-minute AOD differences between AERONET-Cimel (V2 and V3) GAW- and PFR versus optical air mass (m).

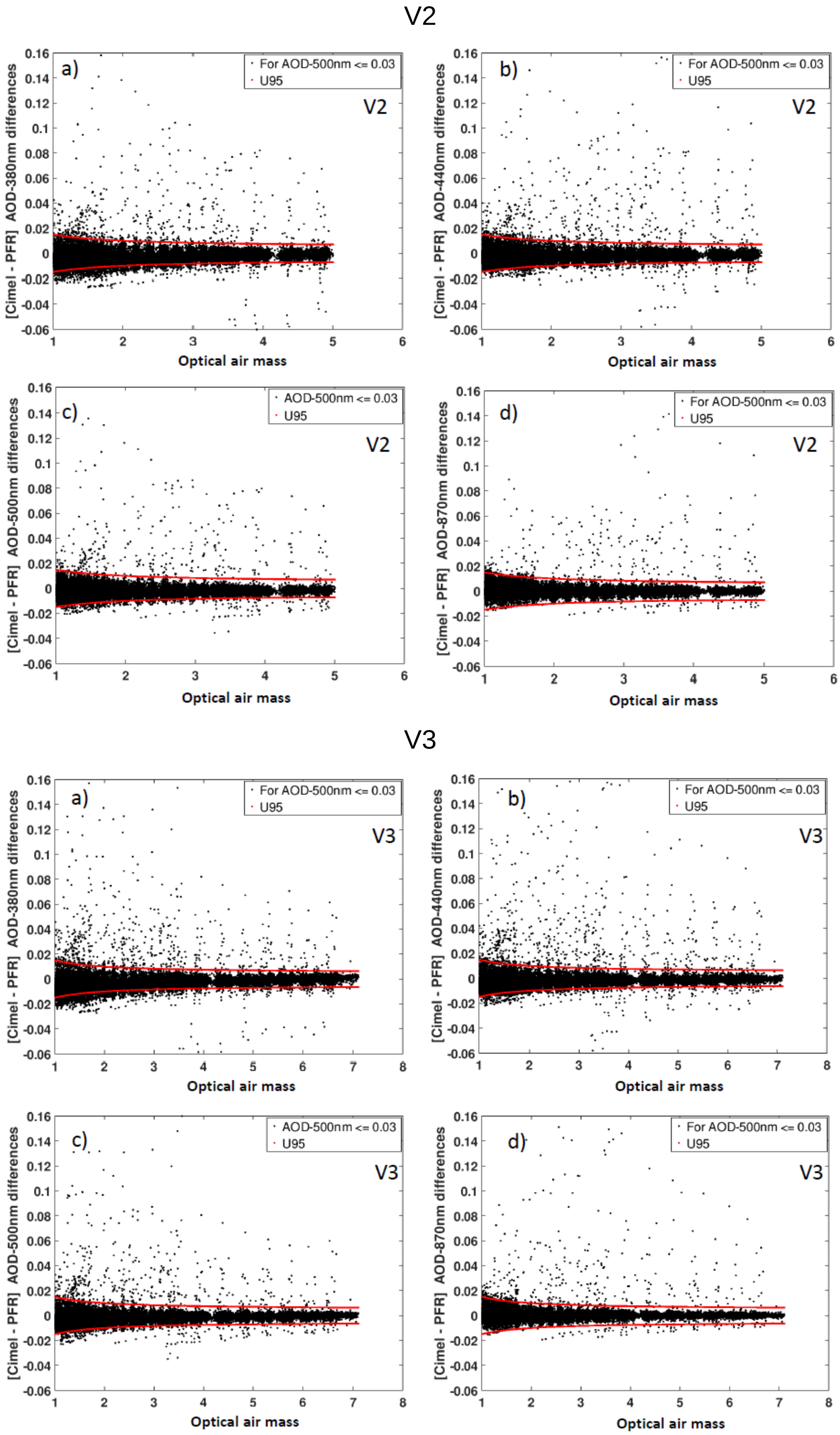

S4. One-minute AOD differences between AERONET-Cimel (V2 and V3) and GAW-PFR versus optical air mass (m) under pristine conditions (AOD_{500nm}≤ 0.03) in the period 2005-2015 for (a) 380 nm, (b) 440 nm, (c) 500 nm and (d) and 870 nm.

Supplement S5. Percentage of [Cimel (V3)-PFR] 1-minute AOD differences meeting the WMO criteria for each wavelength and for different optical air mass.

S5. Percentage of 1-minute AOD data (V3) meeting the WMO criteria for each wavelength for different optical air mass intervals under pristine conditions (AOD_{500nm}≤ 0.03) in the period 2005-2015. This Table is equivalent to Table 7 in the manuscript for AERONET V2.

Percentage of AOD differences within the U95 limits AOD500*nm*≤ 0.03	Total (%)	1 ≤ m < 2 (%)	2 ≤ m < 3 (%)	3 ≤ m < 4 (%)	4 ≤ m < 5 (%)	5 ≤ m < 6 (%)
380 nm	94.9	92.9	95.5	96.7	96.6	96.6
440 nm	97.5	97.2	97.3	98.0	97.6	97.7
500 nm	98.3	98.2	98.2	98.5	98.2	98.3
870 nm	99.0	99.1	99.1	99.1	98.6	98.7

Supplement S6. AOD diurnal range corresponding to AOD outliers under pristine conditions.

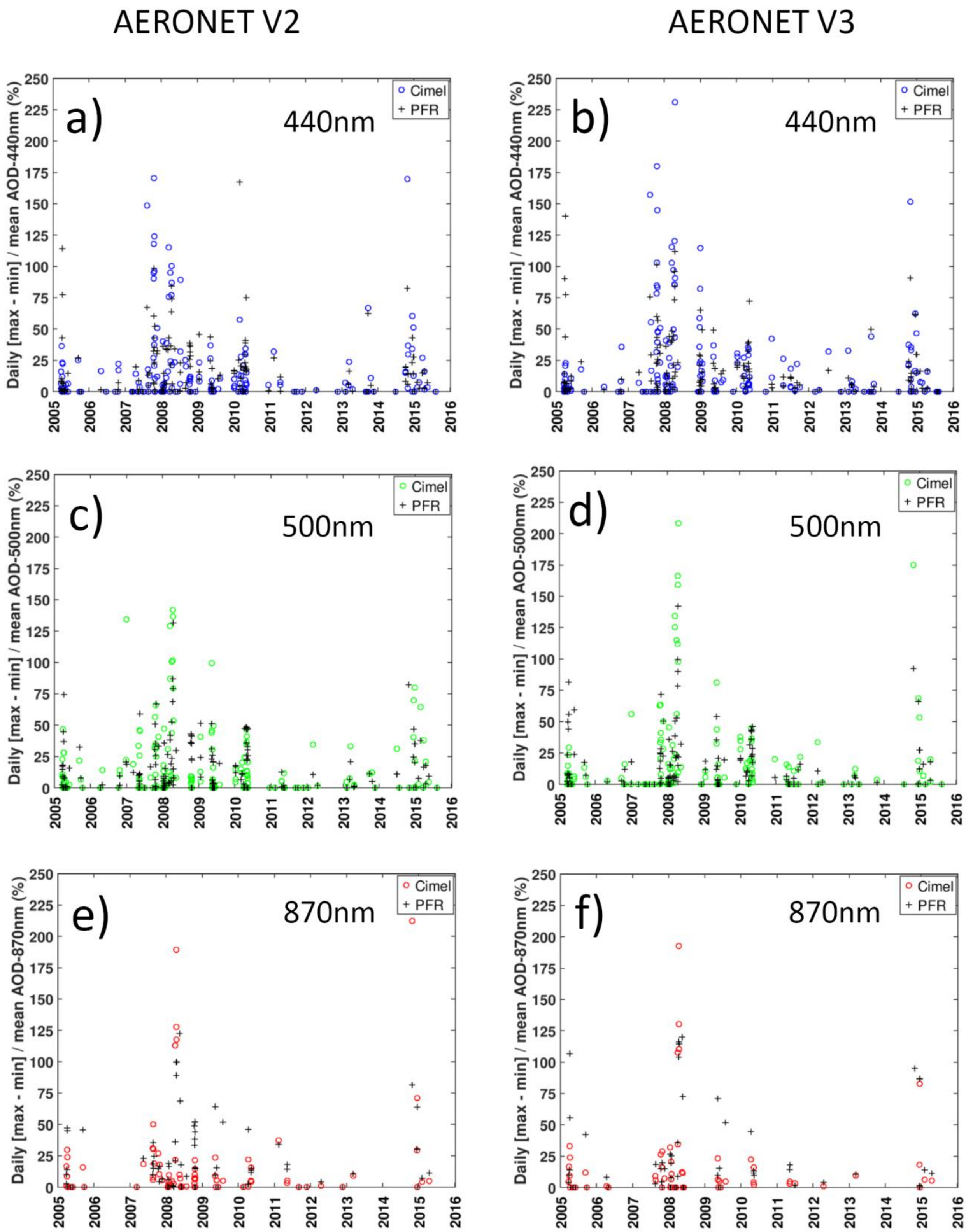

S6. AOD diurnal range variation (maximum value minus minimum value of AOD in one day) corresponding to AOD outliers (non-traceable AOD) under pristine conditions ($AOD_{Cimel-500nm} \leq 0.03$) in the period 2005-2015 for AERONET V2 and V3 and for 440 nm, 500 nm and 870 nm: a) 440 nm V2; b) 440 nm V3; c) 500 nm V2; d) 500 nm V3; e) 870 nm V2; and f) 870 nm V3. This Figure is equivalent to Figure 3 of the manuscript for 380 nm.

Supplement S7. Percentage of AOD_{380nm} outliers of GAW-PFR and AERONET Cimel (V3).

S7. Percentage of cases with AOD_{380nm} outliers of both GAW-PFR and AERONET Cimel (V3) under pristine conditions (Cimel $AOD_{500nm} \leq 0.03$). In these cases the diurnal AOD range was higher than 25% of the daily mean AOD value for which a certain cause has been determined: calibration inaccuracies, cloud screening algorithm failures, mixture of the two previous causes, poor sun pointing, or unknown causes.

	PFR 51 cases	Cimel 81 cases
Calibration inaccuracies	7.8%	44.4%
Cloud screening failures	29.4%	21.0%
Calibration+ cloud screening errors	9.8%	11.1%
Sun misalignments	17.6%	0%
Unknown	35.3%	33.5%

Supplement S8. Examples of fictitious AOD diurnal variation in both GAW-PFR and AERONET-Cimel.

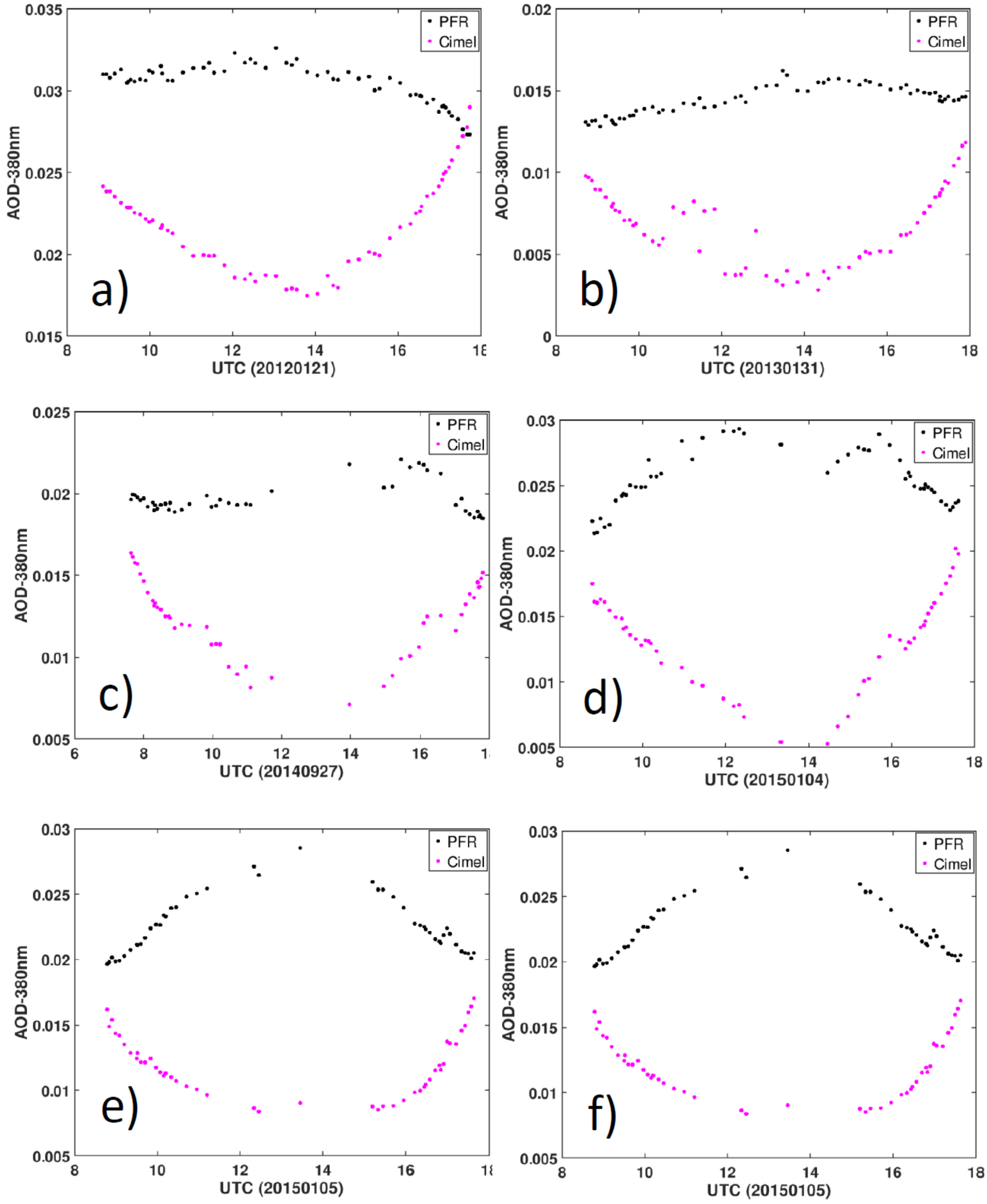

S8. Six examples of fictitious AOD diurnal variation in both GAW-PFR and AERONET-Cimel V3 due to small calibration inaccuracies in the UV channel (368 nm for GAW- PFR and 380 nm for AERONET-Cimel). The date is indicated in the x-axis. In all these cases a clear fictitious AOD diurnal cycle is observed in AERONET-Cimel V3, normally less than 0.01. In cases d), e), and f) an anomalous diurnal cycle is also observed, but in the opposite direction (convex curve), in the case of the GAW-PFR.

These cases reflect a non-perfect calibration in the UV channel and are a cause of non-traceability.

Supplement S9. Examples of AOD diurnal variation of all chanels from AERONET-Cimel Level 2 V3.

The screenshots of AERONET V3 level 2 show that the fictitious diurnal cycle is accentuated, or only clearly observed, in the 340 and 380nm channels.

Screenshots from http://aeronet.gsfc.nasa.gov (last access: 1 february 2019). Izana AERONET station Level 2 Version 3.

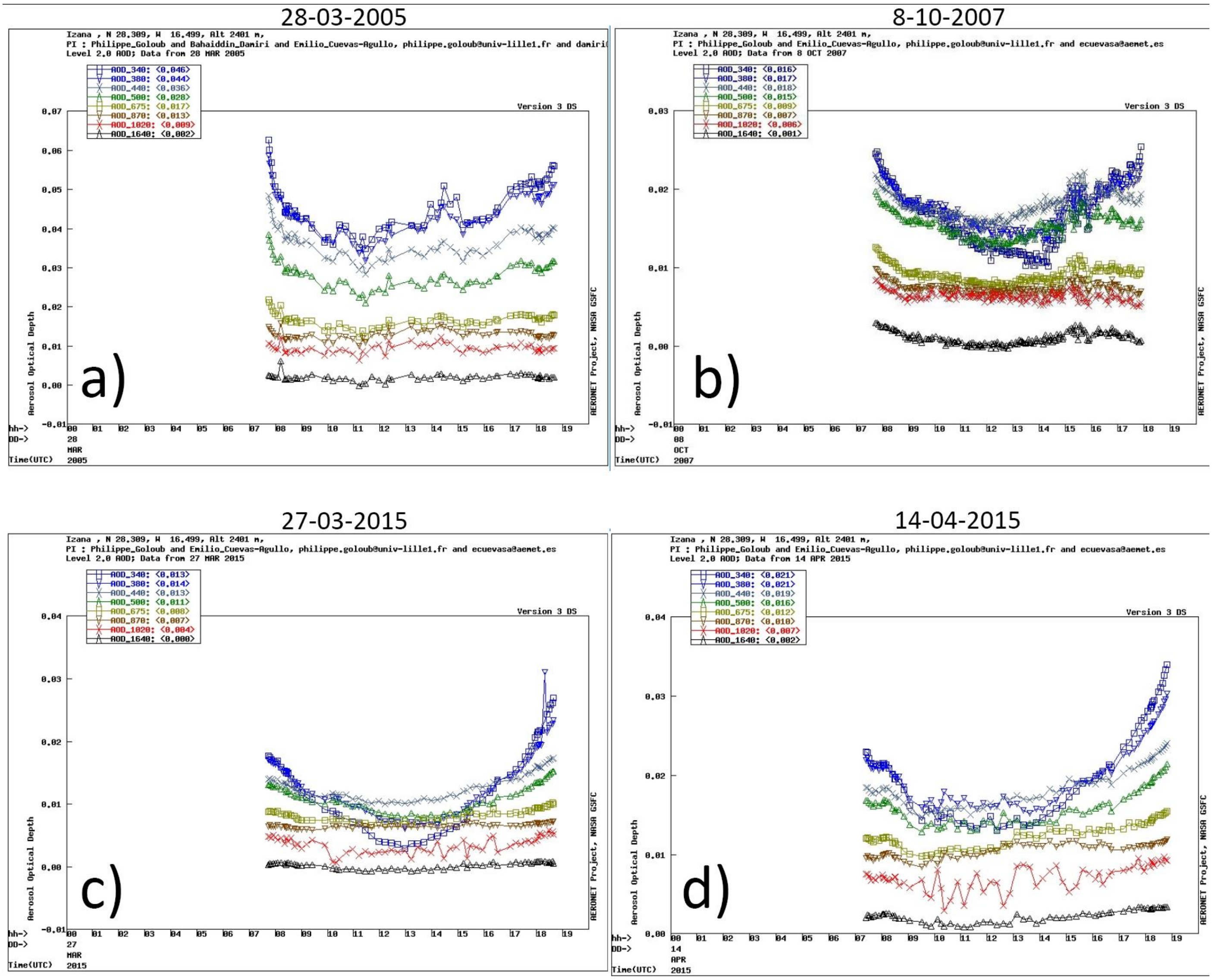

S9. AERONET V3 level 2 AOD Screenshots for all the wavelenghts: a) March 28th, 2005; b) October 8th; 2007; c) March 27th, 2015; and d) April 14th, 2015.

S10. Case analysis of cirrus clouds.

A type of clouds that cause problems in AOD retrieval are the cirrus clouds, usually being present at Izaña between January and April, associated with the presence of the subtropical jet that is normally found in the vicinity of the Canary Islands at this time of year (Rodríguez-Franco and Cuevas, 2013). A constant cloud optical thickness (COT) corresponding to a cloud of a certain horizontal extension would cause the successive measurements within a minute to correspond to the same cloud stage, and therefore it would not be discernible from the extinction caused by aerosols. In the case of very thin cirrus clouds, AOD could increase up to 0.03 (Chew et al., 2011; Giannakaki et al., 2007) with small fluctuations, that cloud-screening algorithms could interpret as the presence of an aerosol layer. Huang et al. (2012) evaluated the impact on AERONET level 2.0 AOD retrievals from cirrus contamination highlighting the difficulties to remove completely their signature, mainly from those subvisual thin cirrus. According to Kinne et al. (1997), optical depth estimates from cirrus derived with sunphotometers have to include forward-scattering effects. Their results show that for cirrus, and instruments with 2.0° and 2.4° FOV, the correction factors vary between 1.6 and 2.5 depending on the crystal size. Taking into account that the FOV of the GAW-PFR is 2.5°, while that of the AERONET-Cimel is 1.3°, such cases will affect the comparison results.

Three case analyses on cirrus clouds are shown below.

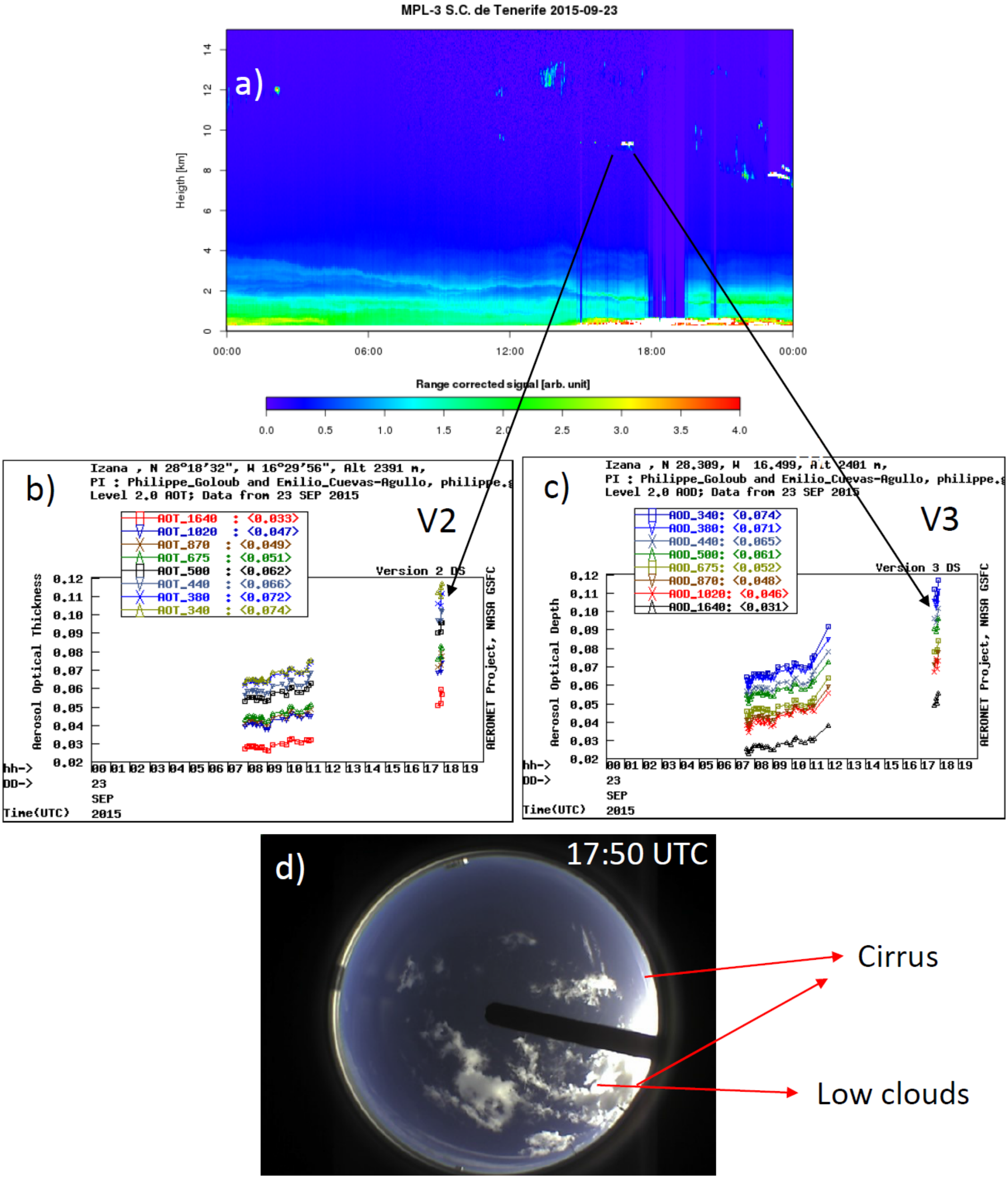

S10.1. Case analysis_September 23, 2015: The range corrected backscattering signal vertical cross section of the Micropulse lidar (MPL) (a) shows scattered cirrus clouds throughout the day (a), and one in particular around 17:45UTC that affects the Cimel AOD measurements. Unfortunately, we do not have measurements for the PFR at this time. The all-sky camera confirms the presence of cirrus clouds at that time (d). The AERONET V2 snapshot registers the impact of the cirrus (b), punctually increasing the AOD values by two. AERONET V3 (c) does not filter these values.

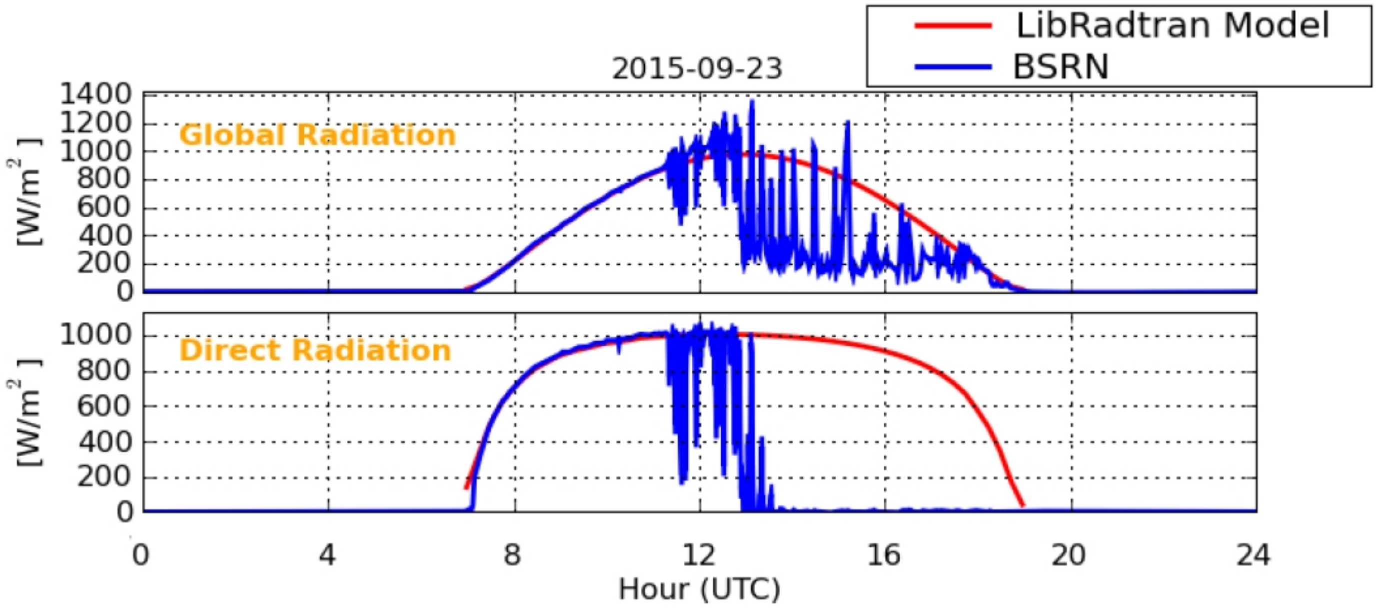

S10.2. Case analysis_September 23, 2015: Global Horizontal (GHI) (top) and Direct Normal Irradiance (DNI) (bottom) from the Surface baseline radiation Network (BSRN) program at Izaña

Global Horizontal (GHI) and Direct Normal Irradiance (DNI) from the Surface Baseline Radiation Network (BSRN) program at Izaña Observatory clearly indicates the presence of clouds in the second half of the day. A high attenuation in DNI from just before 14UTC and during the rest of the day is observed what is not compatible with relatively high AOD measurements at around 17:45UTC (S10.1)

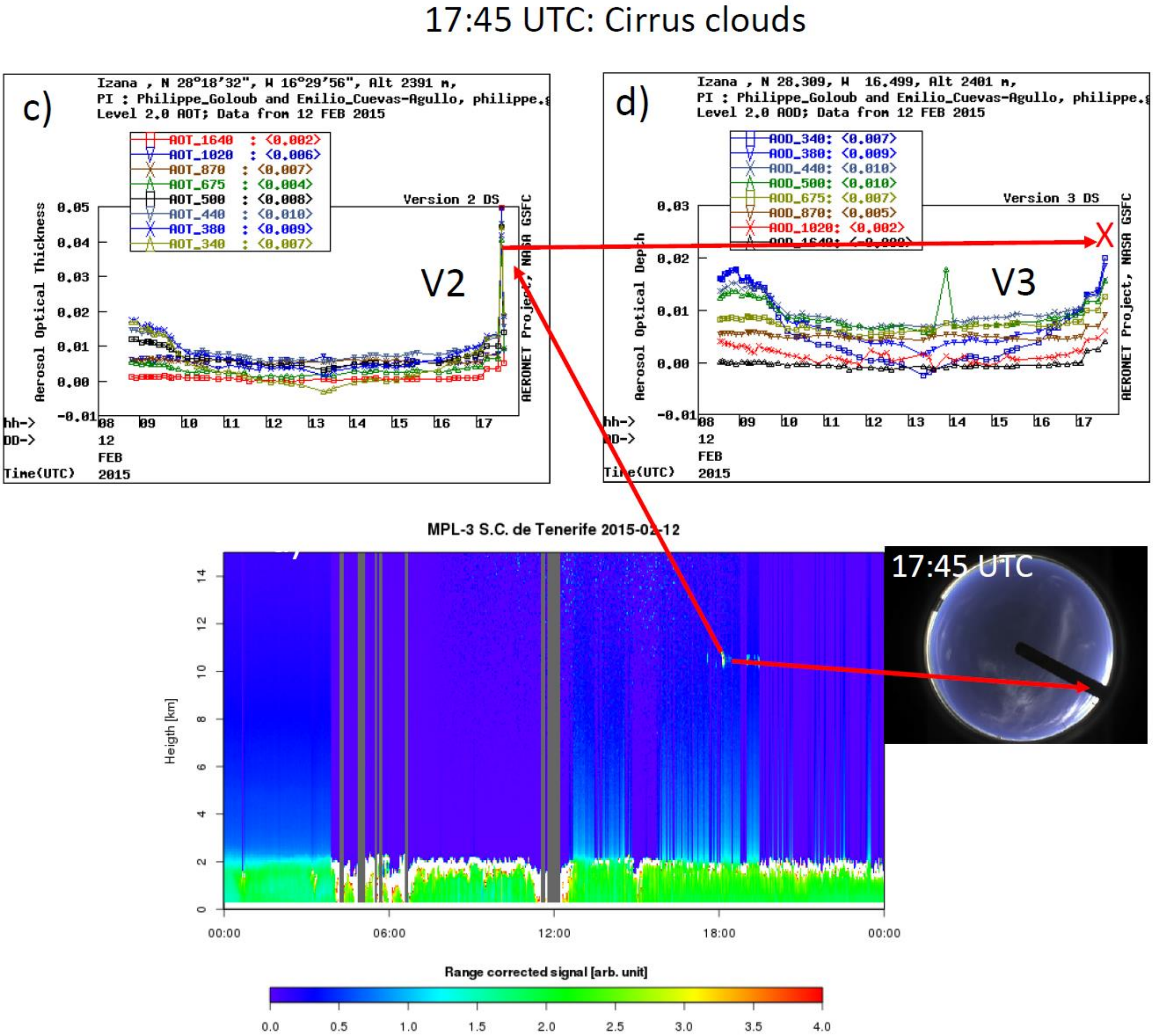

S10.3. Case analysis_February 12, 2015: The range corrected backscattering signal vertical cross section of the Micropulse lidar (MPL) (a) shows the presence of cirrus clouds at around 11 km height between 17:30 and 19:00UTC (a), this is confirmed by the all-sky camera image (b). These cirrus clouds affected the AERONET V2 AOD, increasing the AOD values between 2 and 5 times, depending on the channel (c). AERONET V3 cloud screening correctly filtered these anomalous AOD values (d).

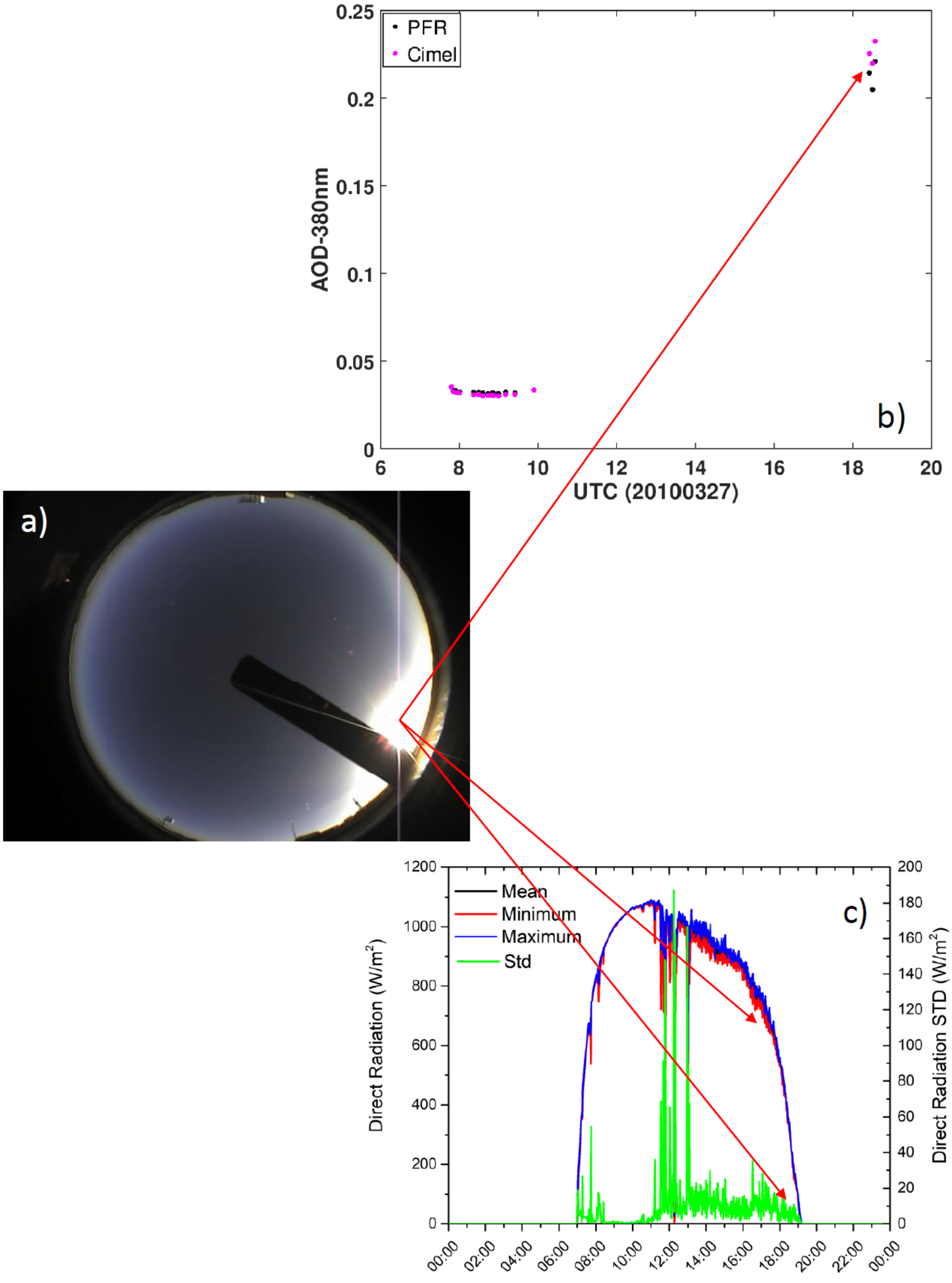

S10.4. Case analysis_March 27, 2010: The cirrus cloud observed by the all-sky camera around 18:30UTC (a) affected both GAW-PFR and AERONET V3, giving AOD values about 8 times higher than those observed early in the morning (b). The erroneous AOD values of the GAW-PFR are slightly lower than those of AERONET V3. The cause could be a greater forward-scattering effect of the cirrus cloud on the GAW-PFR due to its higher FOV (compared with that of the Cimel). The presence of cirrus has been confirmed with the direct normal irradiance records (c) that shows a typical noisy signal (relatively high standard deviation) until 19 UTC.

Supplement S11. Impact of low stratocumulus on AOD retrieval.

Another cloud scenario that can affect AOD traceability is the presence of low clouds (stratocumulus) that sometimes exceed the observatory height level because the temperature inversion is around 2400 m height.

The selected case analysis is really interesting. Moreover, it is representative of a relatively frequent situation in winter, when the temperature inversion is very close to the altitude of the Izaña Observatory.

The Modis image of that day (S11.1a) shows a large part of the island of Tenerife covered with stratocumulus except in its central part corresponding to the summits of the island (2400 m a.s.l. plateau) in whose NE limit the Izaña Observatory is located. This is confirmed by the range corrected backscattering signal vertical cross section of the Micropulse lidar (MPL) (S11.1b) indicating a quasi-permanent stratocumulus layer above 2000 m a.s.l. throughout the day. In these cases, the appearance of intermittent fog banks in the Observatory or on the horizon (S11.1c), in its vicinity, is very common.

The AOD outliers measured by the PFR around 08:00 UTC (S11.1d) are due precisely to these intermittent fog blanks on the horizon and/or above Izaña Observatory. In S11.2 we can see a sequence of all-sky images from 07:30 UTC. Although the all-sky camera records some frozen ice on its dome, it does not appear in the sunlit part. The PFR external lens were free of frozen ice all the time. From the all-sky camera imagery, the presence of fog from around 08:00 UTC to 09:00 UTC is observed. This is confirmed with DNI and other radiation-components measurements (S11.3). Early morning fog veils caused erroneous AOD values from PFR but not from Cimel. The explanation is in the measurement mode. As the sky conditions changes are very fast under intermittent fog blanks, the 1-second measurements (at 1-minute intervals) of the PFR may not capture this AOD variation, while the triplets of the Cimel (3 consecutive 1-second measurements) might do so, correctly functioning the cloud screening in this case.

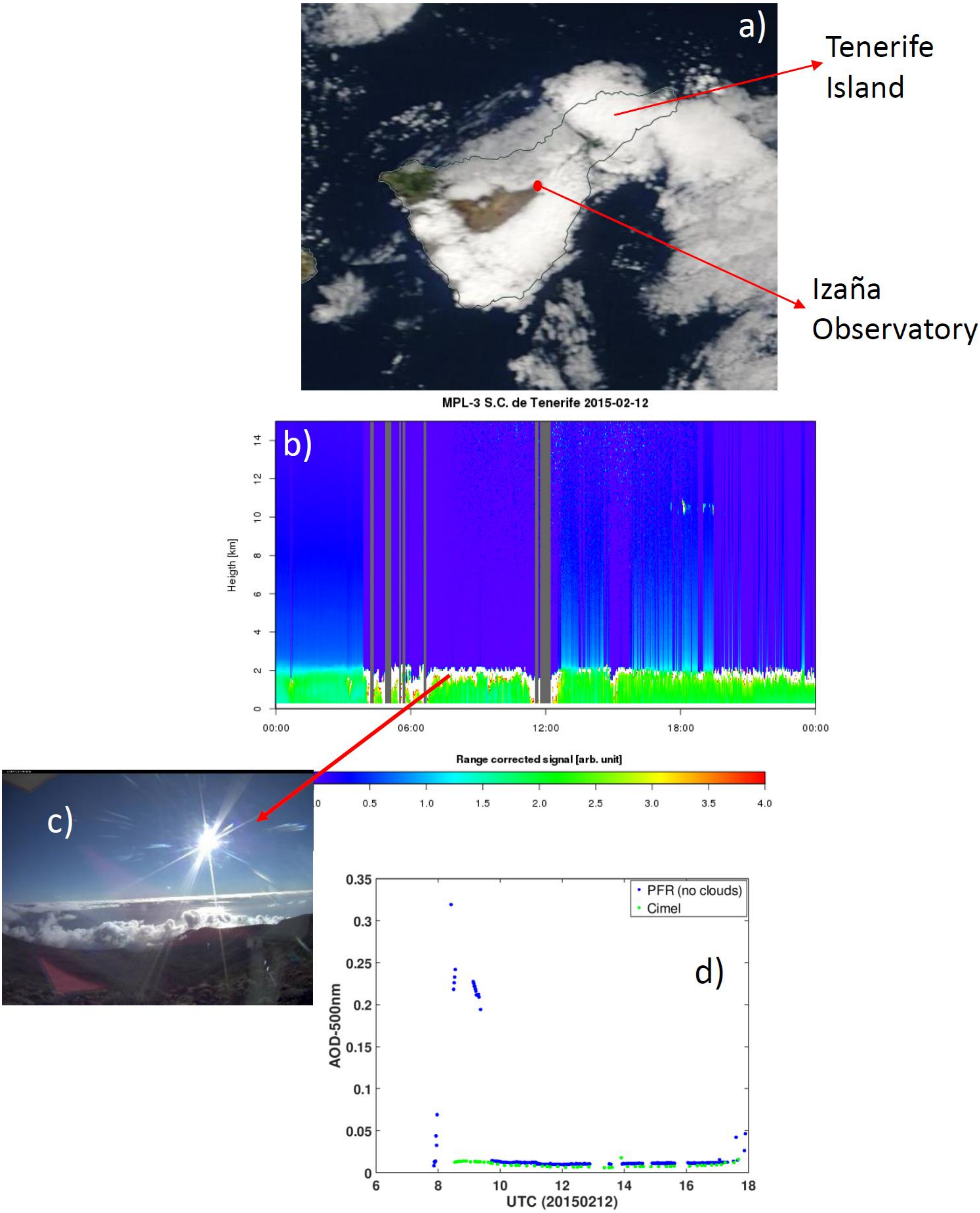

S11.1. February 12, 2015: Modis visible image; the range corrected backscattering signal vertical cross section of the Micropulse lidar (MPL) (b);East facing webcam picture around 09:00UTC; PFR and Cimel AOD (d).

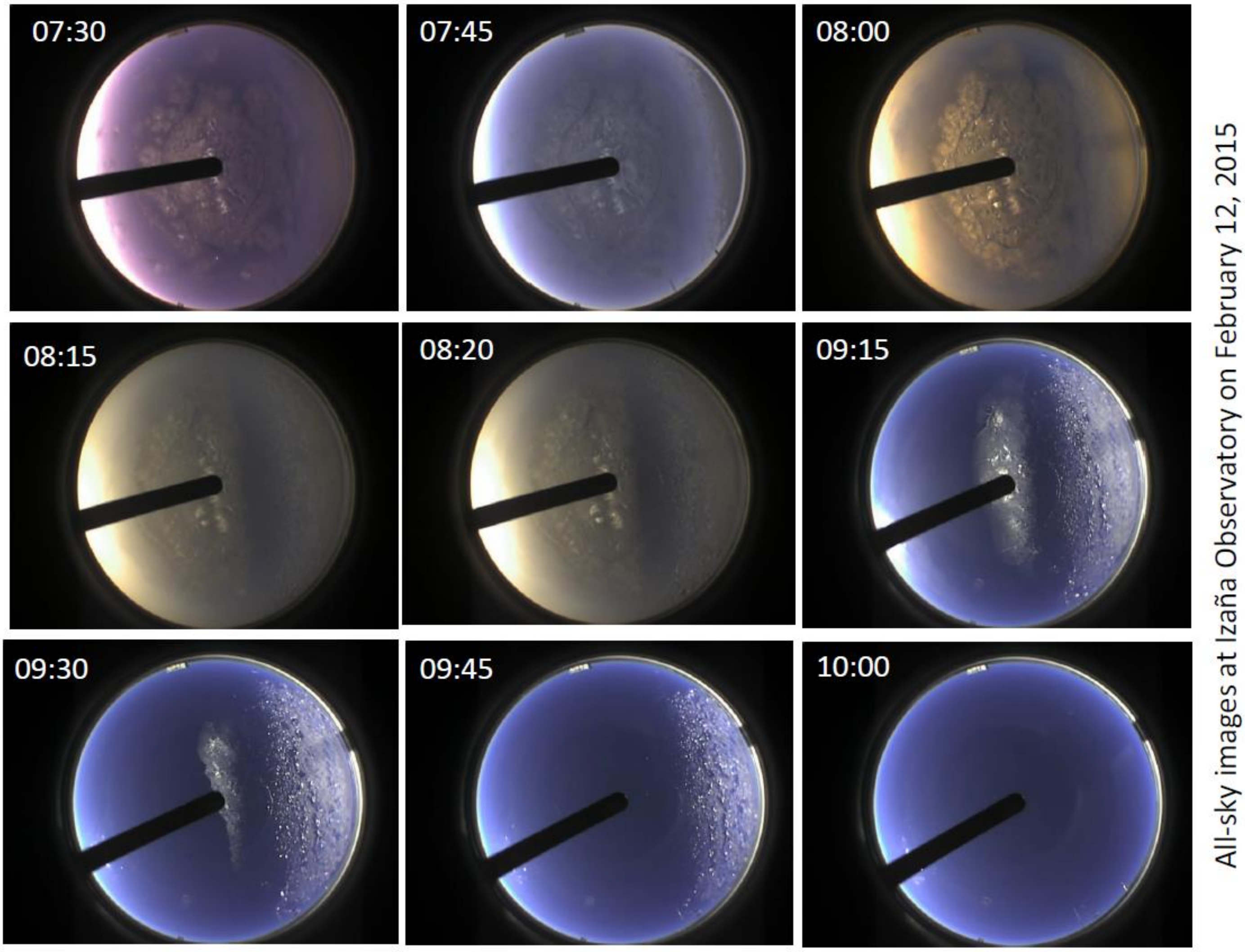

S11.2. All-sky images sequence on February 12, 2015.

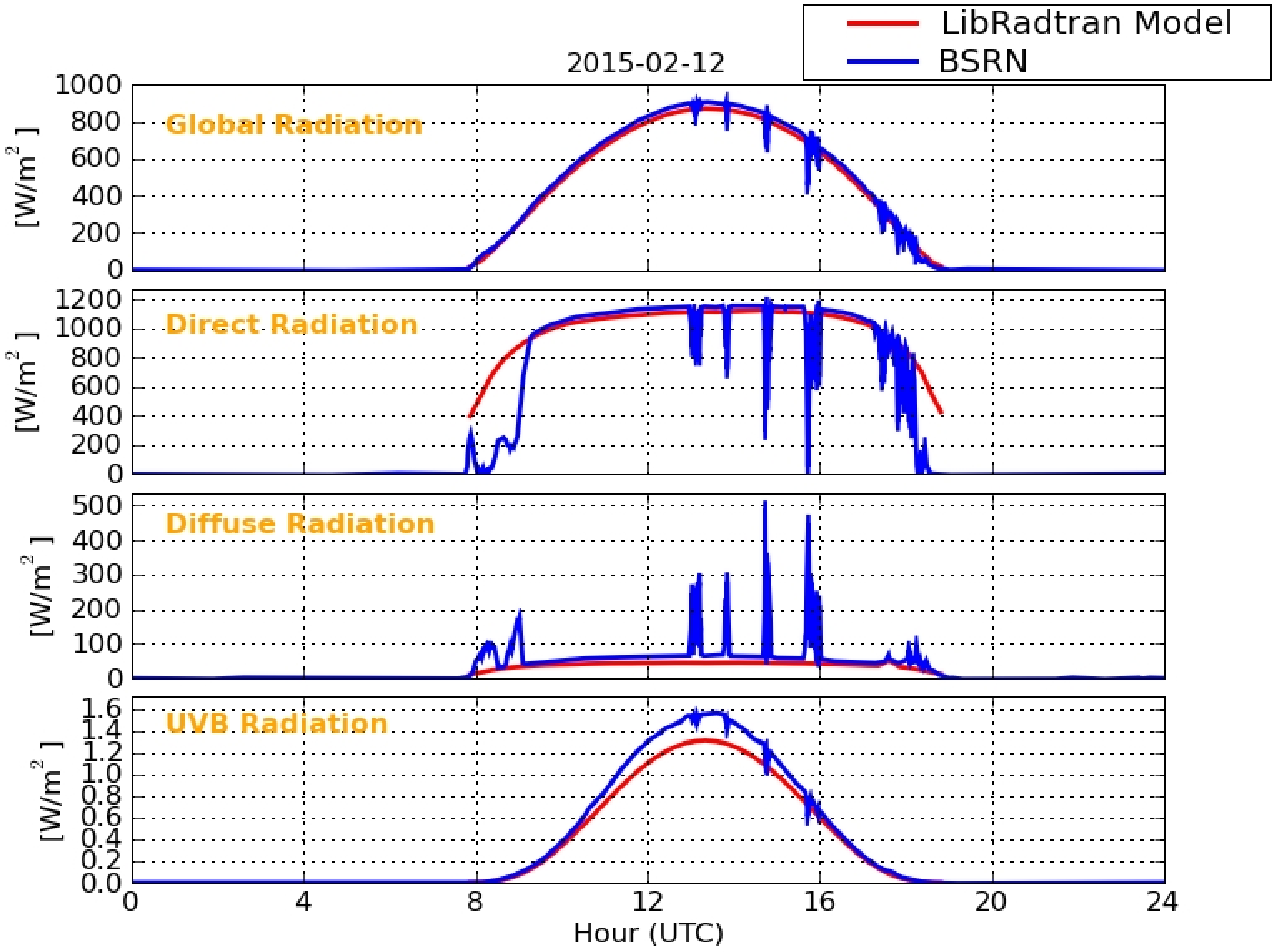

S11.3. Global Horizontal (GHI), Direct Normal Irradiance (DNI), Difuse Horizontal Irradiance (DHI) and UVB radiation from the Surface Baseline Radiation Network (BSRN) program at Izaña Observatory on February 12, 2015.

Supplement S12. Actual AOD differences between AERONET-Cimel V3 and GAW-PFR vs PFR AOD

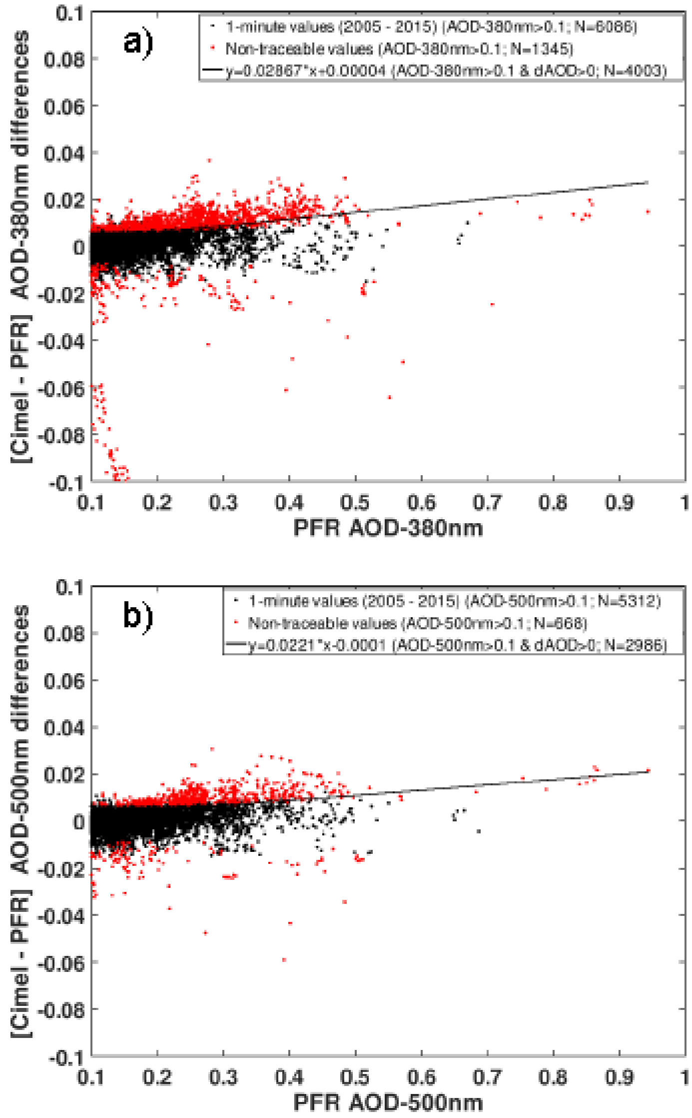

S12. Actual AOD differences between AERONET-Cimel V3 and GAW-PFR vs PFR AOD at (a) 380 nm (b) and 500 nm for the period 2005-2015. The fitting line has been calculated with AOD data > 0.1 and Cimel-PFR AOD difference > 0. Number of data used in the plots are indicated in the legend. The percentage of non-traceable AOD data with these conditions is ~22% for 380nm, and ~13% for 500nm. Note that some traceable (black) points show larger AOD differences than non-traceable (red) points because of air mass dependence of the WMO traceability criterion.

Supplement S13. Percentage of AERONET V3 AOD data outside the U95 limits for high AOD conditions

S13. Percentage of AERONET V3 AOD data outside the U95 limits at 380 nm, 440 nm, 500 nm and 870 nm channels and for three AOD_{500nm} thresholds with respect to all data and with respect to all data for each AOD interval (in brackets).

	Percentage of AOD data outside the $U95$ limits (%)		
	$AOD_{500nm} > 0.1$	$AOD_{500nm} > 0.2$	$AOD_{500nm} > 0.3$
380 nm	1.6 (22.9)	1.1 (42.0)	0.4 (54.4)
440 nm	1.1 (15.9)	0.9 (32.5)	0.4 (49.0)
500 nm	1.3 (18.4)	1.0 (37.6)	0.5 (55.7)
870 nm	0.5 (6.7)	0.4 (13.4)	0.2 (19.0)

Comparing versions V2 and V3, we can see that, except for the 380 nm channel, in V3 the non-AOD traceability increases with respect to that found in V2.

Supplement S14. Simulations of scattered to direct radiation simulations.

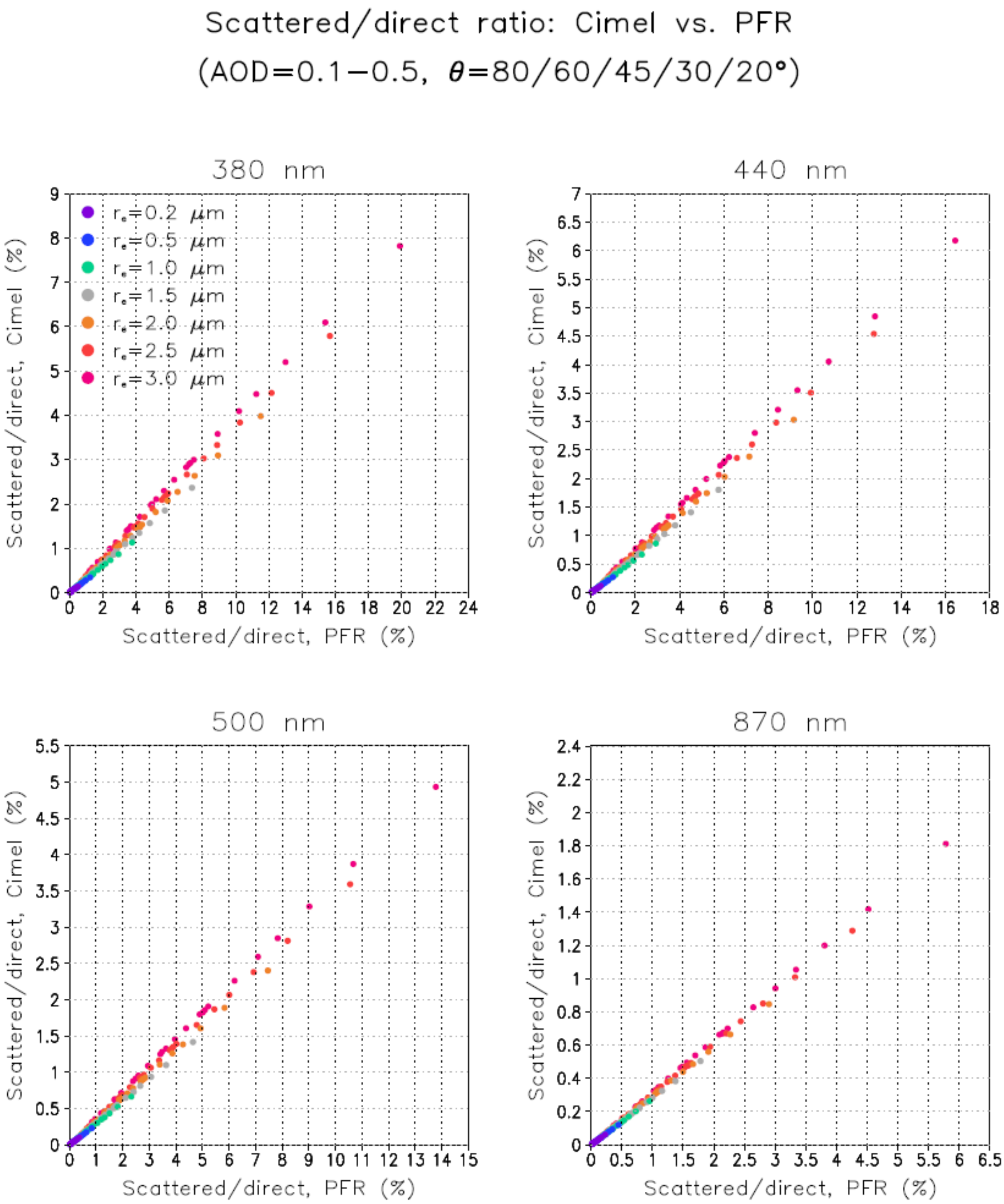

S14. Scattered to direct radiation simulations made with a forward Monte Carlo model (Barker 1992, Barker 1996, Räisänen et al. 2003) for FOVs of 2.5° and 1.2° for seven values of effective radius (r_e=0.2, 0.5, 1.0, 1.5, 2.0, 2.5, and 3.0 μm), for five AOD values (AOD= 0.1, 0.2, 0.3, 0.4, and 0.5), and for five solar zenith angles (θ = 20°, 30°, 45°, 60° and 80°).

Supplement S15. Relative error in AOD for PFR and Cimel.

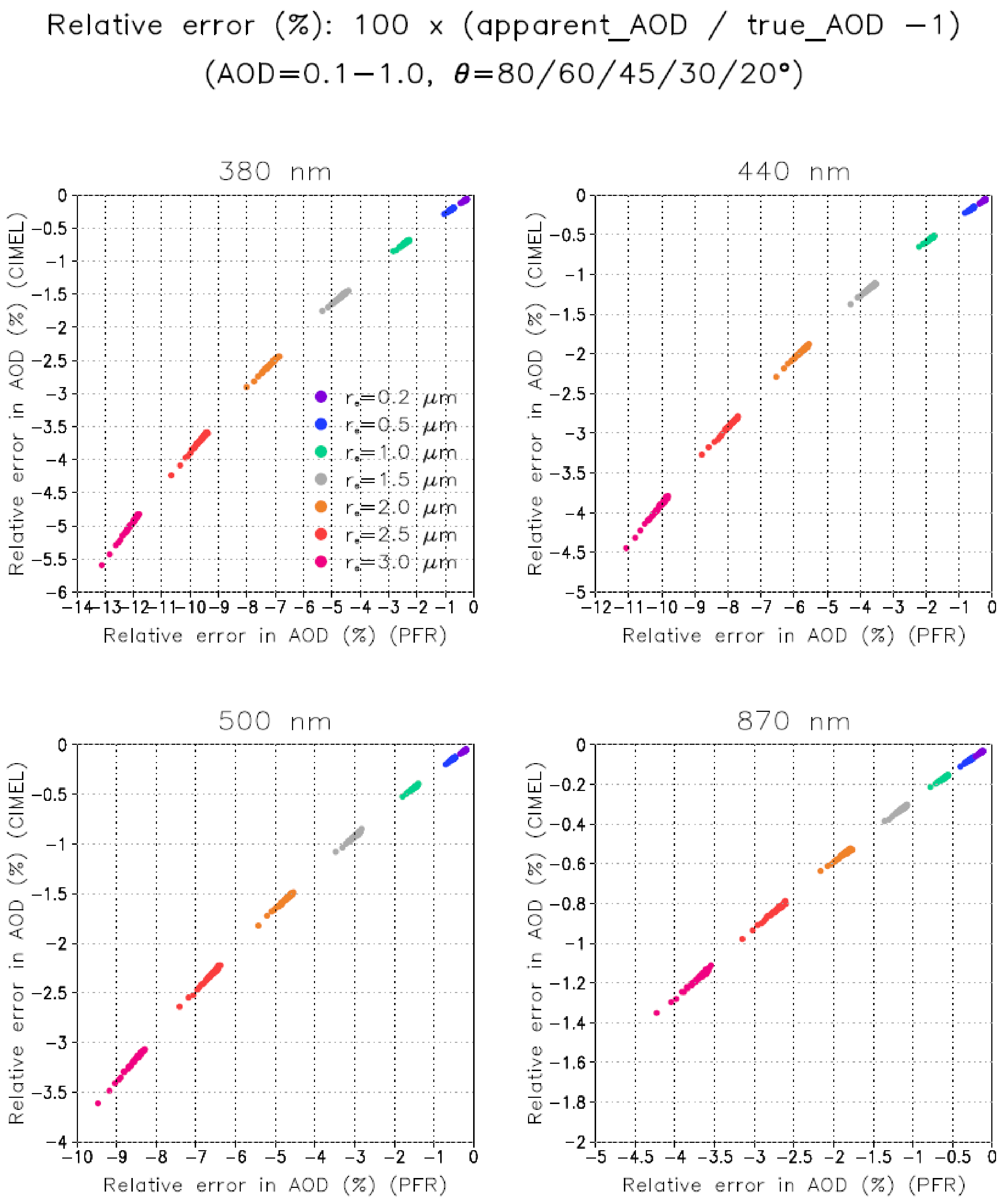

S15. Relative error in AOD for PFR (x-axis) and Cimel (y-axis) for seven values of effective radius (r_e=0.2, 0.5, 1.0, 1.5, 2.0, 2.5 and 3.0 μm), for five AOD values (AOD= 0.1, 0.2, 0.3, 0.4, and 0.5), and for five solar zenith angles (θ = 20°, 30°, 45°, 60° and 80°).

<u>**Supplement S16. Actual AOD differences between AERONET-Cimel V3 and GAW-PFR vs PFR AOD after AOD_{PFR} correction.**</u>

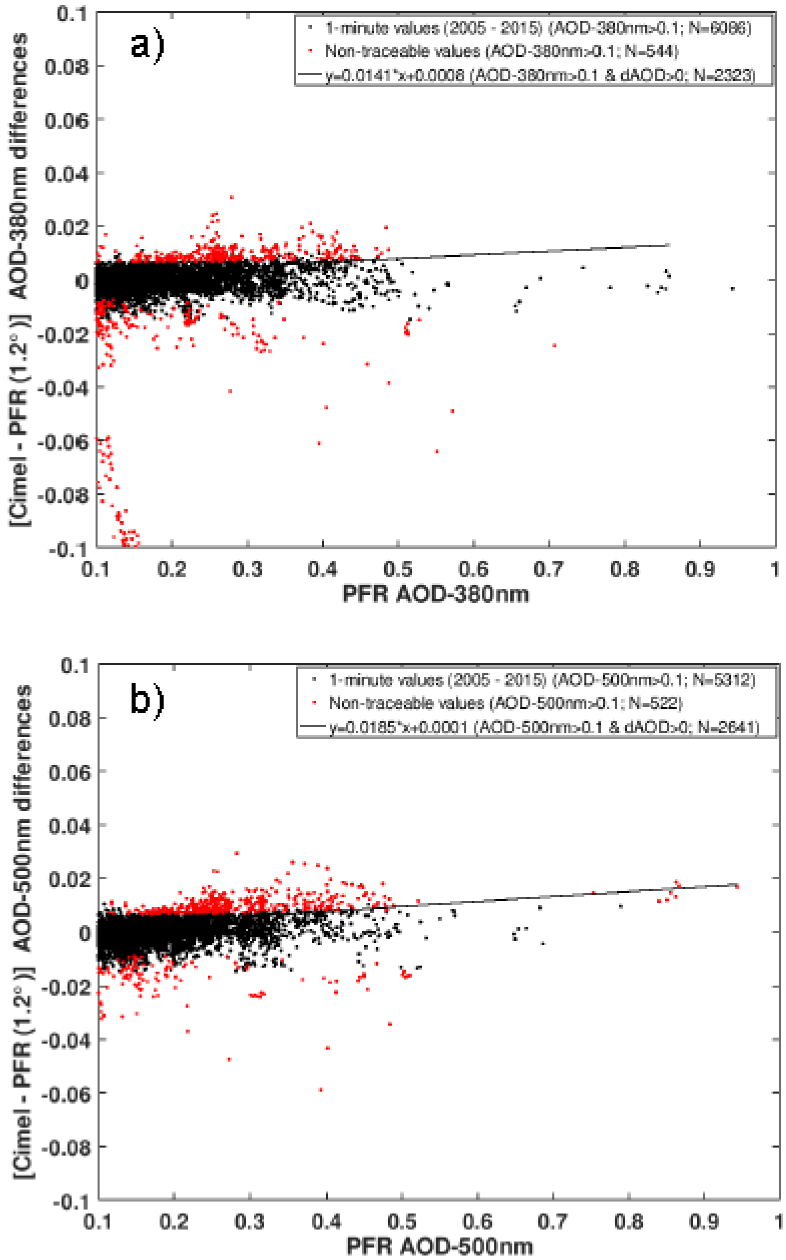

S16. The same as the Figure of Supplement S13 (AERONET V3) after the PFR AOD data were "corrected" by adding + 3.3% at 380nm and + 2.2.% at 500 nm to the 1-minute AOD PFR data > 0.1.

Supplement S17. Ångström exponent comparison

This basic statistic indicates the degree of agreement between GAW-PFR and AERONET-Cimel in the aerosol "characterization" in the long term using only AE. Therefore, we did not include AOD as it would have been strictly necessary to carry out a proper characterization of the aerosol types present in a specific site. The four chosen categories are very close to the real ones at Izaña but without including AOD. What is relevant here in is not the chosen categories, but the degree of agreement that both radiometers have to provide the same aerosol category according to the AE. This requires a very high simultaneous agreement in AOD in the four channels.

a)

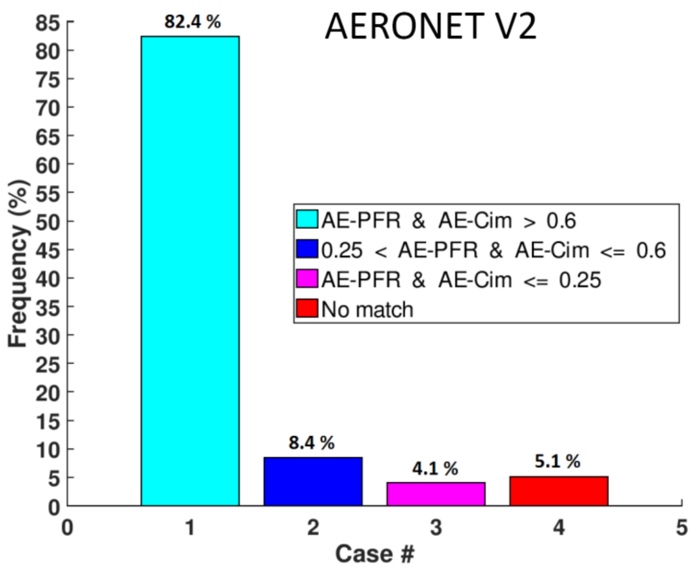

b)

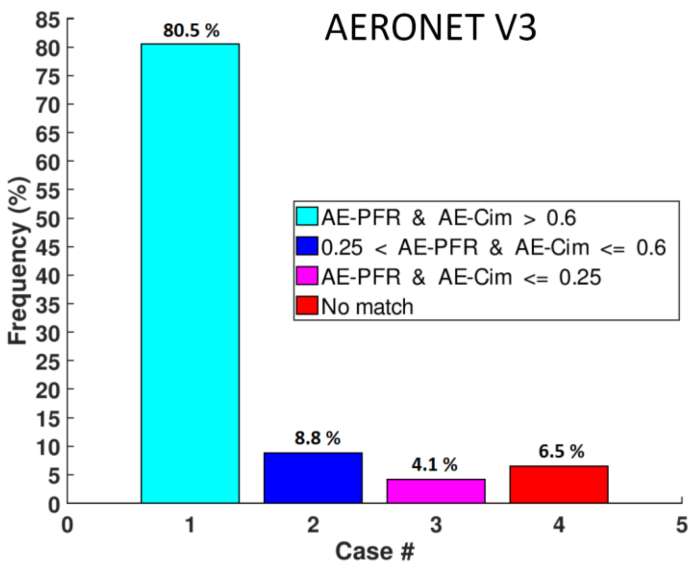

S.17. Percentage of cases in which GAW PFR and AERONET V2 (a) and V3 (b) coincide in each AE scenario (period 2005-2015).

References

Chew, B. N., Campbell, J.R., Reid, J.S., Giles, D.M., Welton, E.J., Salinas, S.V., and Liew, S.C.: Tropical cirrus cloud contamination in sun photometer data, Atmos. Environ., 45, 6724-6731. 10.1016/j.atmosenv.2011.08.017, 2011.

Giannakaki, E., Balis, D. S., Amiridis, V., and Kazadzis, S.: Optical and geometrical characteristics of cirrus clouds over a Southern European lidar station, Atmos. Chem. Phys., 7, 5519-5530, https://doi.org/10.5194/acp-7-5519-2007, 2007.

Huang, J., Hsu, N.C., Tsay, S.-C., Holben, B.N., Welton, E.J., Smirnov, A., Jeong, M.-J., Hansell, R.A., Berkoff, T.A., Liu, Z., Liu, G.-R., Campbell, J.R., Liew, S.C., and Barnes, J.E.: Evaluations of cirrus contamination and screening in ground aerosol observations using collocated lidar systems, J. Geophys. Res., 117, D15204, doi:10.1029/2012JD017757, 2012.

Kinne, S., Akerman, T. P., Shiobara, M., Uchiyama, A., Heymsfield, A. J., Miloshevich, L., Wendell, J., Eloranta, E., Purgold, C., and Bergstrom, R. W.: Cirrus cloud radiative and microphysical properties from ground observations and in situ measurements during FIRE 1991 and their application to exhibit problems in cirrus solar radiative transfer modeling, J. Atmos. Sci., 54, 2320–2344, https://doi.org/10.1175/1520-0469(1997)054<2320:CCRAMP>2.0.CO;2, 1997.

Rodriguez-Franco, J. J., and Cuevas, E.: Characteristics of the subtropical tropopause region based on long-term highly-resolved sonde records over Tenerife, J. Geophys. Res. Atmos., 118, doi:10.1002/jgrd.50839, 2013.